Electronic Supplementary Material (ESI) for Physical Chemistry Chemical Physics.
This journal is © the Owner Societies 2020

Electronic Supplementary Information

Graphdiyne coordinated transition metals as single-atom catalysts for nitrogen fixation

Zhen Feng,[a, b] Yanan Tang,[*c] Weiguang Chen,[c] Yi Li,[b] Renyi Li,[b] Yaqiang Ma,[b] and Xianqi Dai [*b]

Contents

[a] School of Materials Science and Engineering, Henan Institute of Technology, Xinxiang, Henan 453000, China.

[b] School of Physics, Henan Normal University, Xinxiang, Henan 453007, China. E-mail: xqdai@htu.cn

[c] College of Physics and Electronic Engineering, Zhengzhou Normal University, Zhengzhou 450044, China. E-mail: yntang2010@163.com

Supplementary Figures

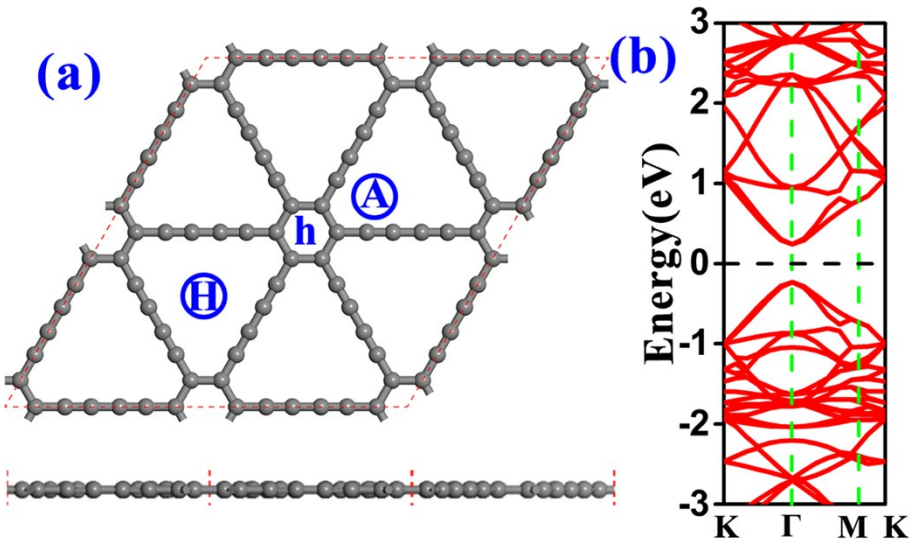

Fig. S1. (a) Structure of the pristine GDY monolayer (2×2) supercell with the considered adsorption sites for the single metal atoms. The gray balls represent C atoms. (b) Band structure of the pristine GDY monolayer. The Fermi level is set to 0 eV.

The geometries of GDY monolayer were relaxed, as shown in **Fig. S1(a)**, the optimized lattice constants of GDY is 9.44 Å. **Fig. S1(b)** showes that the pristine GDY exhibits the semiconductor with a direct band gap (E_{gap}) of 0.47 eV.

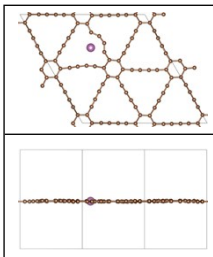	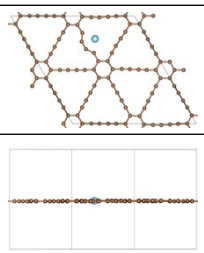	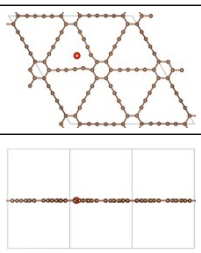	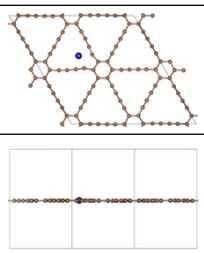	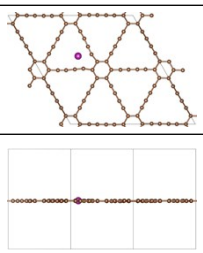
Sc@GDY	Ti@GDY	V@GDY	Cr@GDY	Mn@GDY
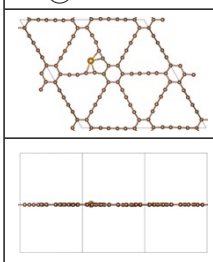	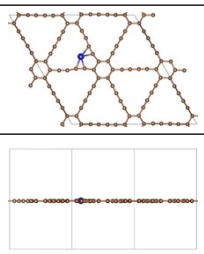	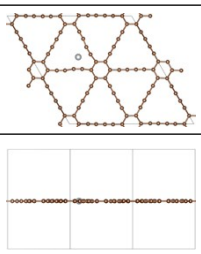	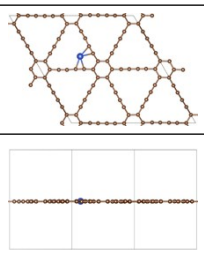	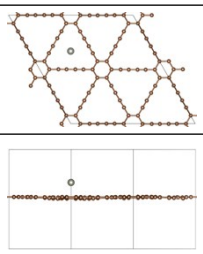
Fe@GDY	Co@GDY	Ni@GDY	Cu@GDY	Zn@GDY
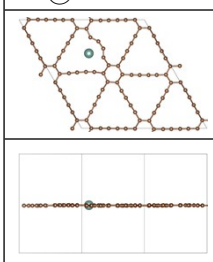	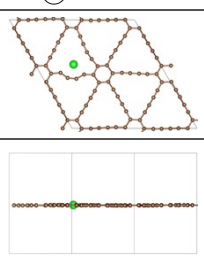	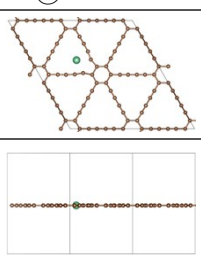	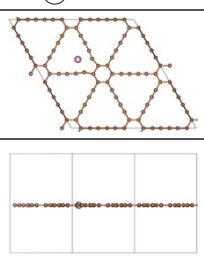	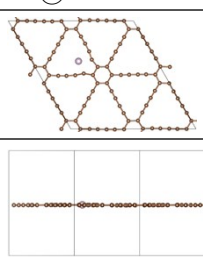
Y@GDY	Zr@GDY	Nb@GDY	Mo@GDY	Tc@GDY
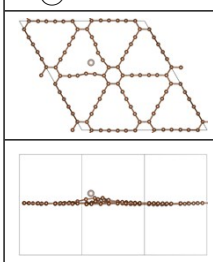	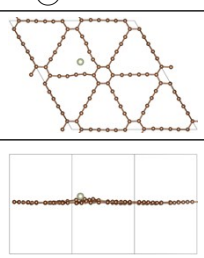	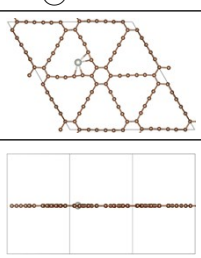	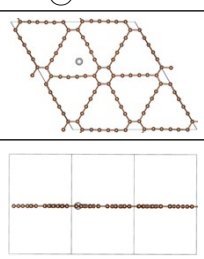	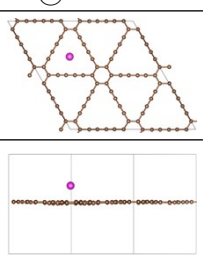
Ru@GDY	Rh@GDY	Pd@GDY	Ag@GDY	Cd@GDY
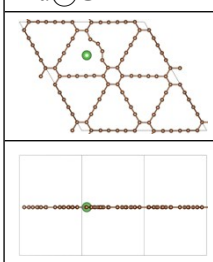	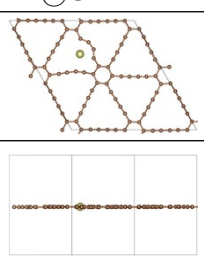	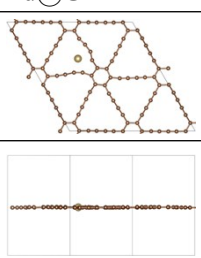	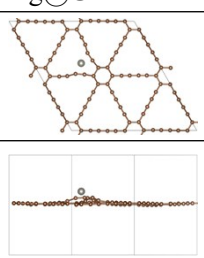	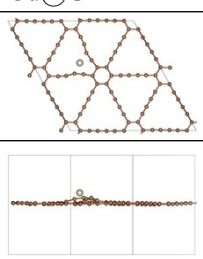
La@GDY	Hf@GDY	Ta@GDY	W@GDY	Re@GDY
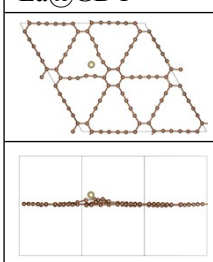	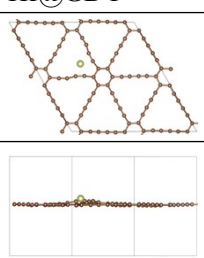	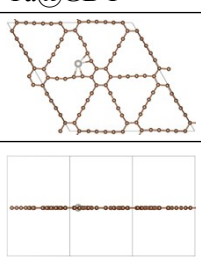	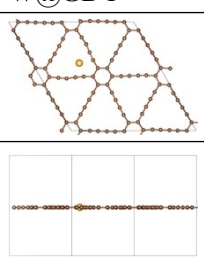	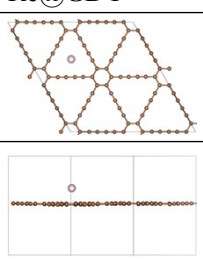
Os@GDY	Ir@GDY	Pt@GDY	Au@GDY	Hg@GDY

Fig. S2. Optimized stable geometries of TM@GDY sheets. The brown and color balls represent C and TM atoms, respectively.

The binding sites of TM and GDY can be divided into three types. The Sc, Ti, Sc, Ti, Y, Zr, La and Hf atom are anchored next to acetylene linkage; The captured Zn, Cd and Hg atom are located above the surface of GDY with a distance of 2.436 Å, 2.668 Å, 2.397 Å, respectively; The other atoms are anchored at the corner of 18 C-hexagon.

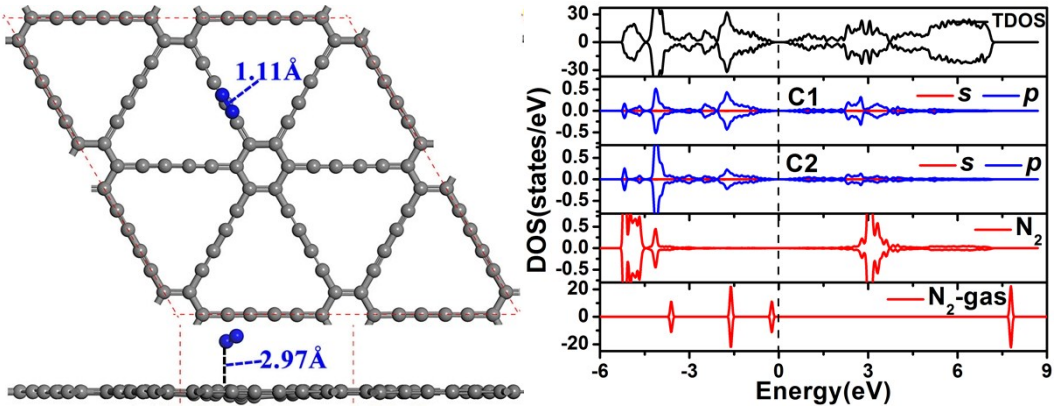

(a) (b)

Fig. S3. (a) Optimized configuration of N_2 molecule adsorbed on pristine GDY. (b) Density of state (DOS) of the N_2/GDY systems. The energy zero is taken as the Fermi level.

As shown in **Fig. S3**, the distance between the N_2 and the GDY plane is 2.97 Å, the corresponding N-N bond length is the same as isolated N_2 molecule (1.11 Å), and the adsorption energy is -0.07 eV, which indicates that the N_2 is physisorbed on GDY surface.[2] Therefore, the pristine GDY do not capture N_2 molecules efficiently.

Systems	*N_2 side	*N_2 end	Systems	*N_2 side	*N_2 end
Sc@GDY	-	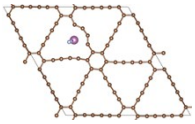	Ti@GDY	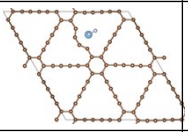	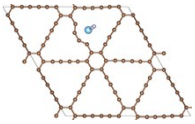
	-	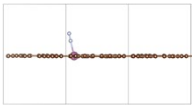		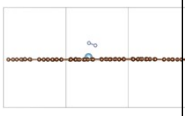	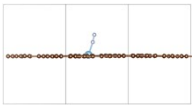
V@GDY	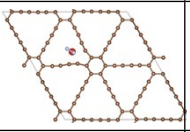	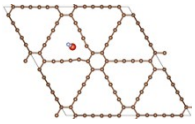	Cr@GDY	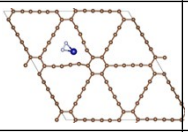	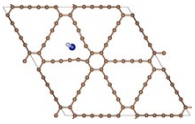
	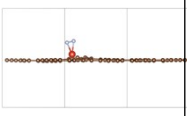			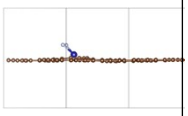	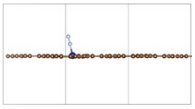
Mn@GDY	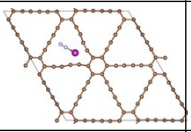	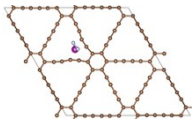	Fe@GDY	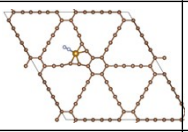	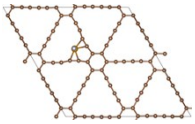
	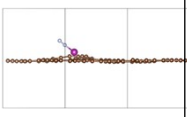	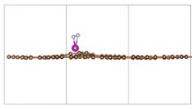		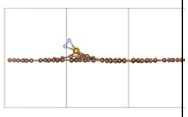	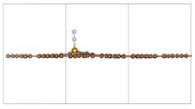
Co@GDY	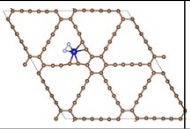	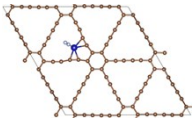	Ni@GDY	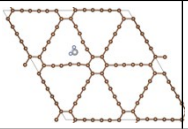	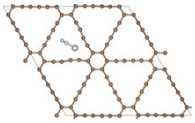
	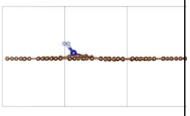	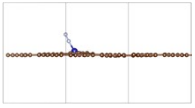		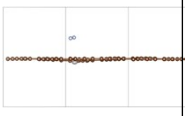	
Cu@GDY	-	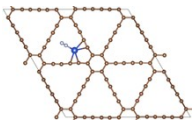	Y@GDY	-	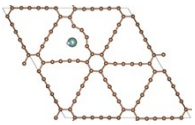
	-	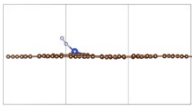		-	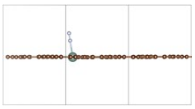
Zr@GDY	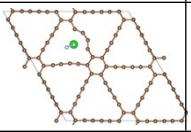	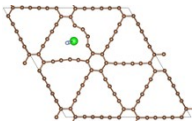	Rh@GDY	-	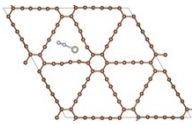
	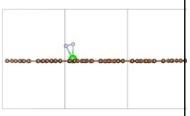	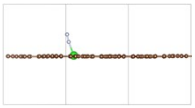		-	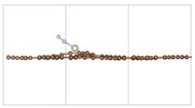
Pd@GDY	-	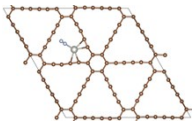	Ag@GDY	-	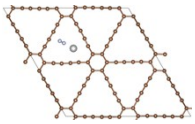

	-	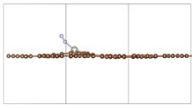		-	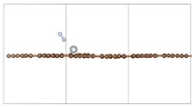
La@GDY	-	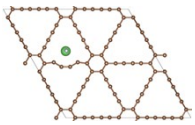	Hf@GDY	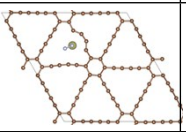	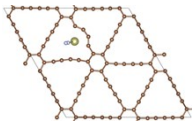
	-	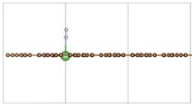		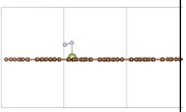	
Pt@GDY	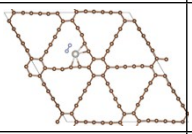	-	-	-	-
	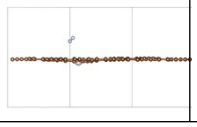	-	-	-	-

Fig. S4. Optimized geometries of N_2 adsorption on various TM@GDY sheets. The brown, blue, and color balls represent C, N, and TM atoms, respectively.

The adsorption of N_2 molecule on various TM@GDY surfaces was evaluated with different configurations (side-on and end-on) and adsorption sites.[1] For TM@GDY (TM=Sc, Cu, Y, Rh, Pd, Ag, La), the side on configurations transfer to end on configurations, while both side-on and end-on configurations can exist when TM= Ti, V, Cr, Mn, Fe, Co, Ni, Zr, Hf.

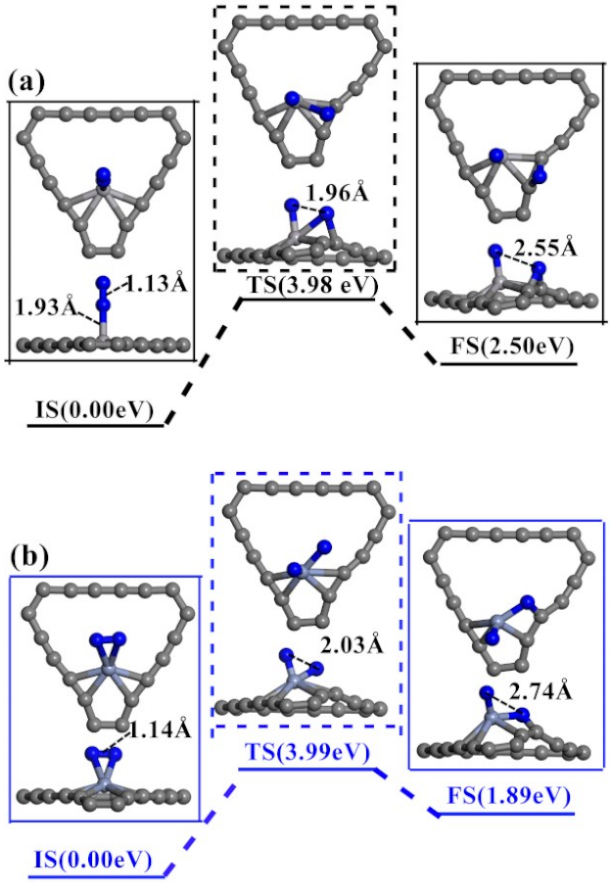

Fig. S5. The N_2 molecule dissociation pathway on (a) V@GDY and (b) Cr@GDY. The gray and blue balls represent C and N atoms.

Fig. S5 shows $*N_2 \rightarrow *N + *N$ dissociation reactions on V@GDY and Cr@GDY surfaces. The reactions require to overcome a very high energy barrier of 3.98~3.99 eV and are endothermic process with large reaction energy of 2.50 eV and 1.89 eV for V@GDY and Cr@GDY, indicates that direct dissociation of N_2 into two separated N atoms on TM@GDY monolayer is still hard to occur. Thereby, the N_2 associative pathway is selected to further study and discuss in detail.

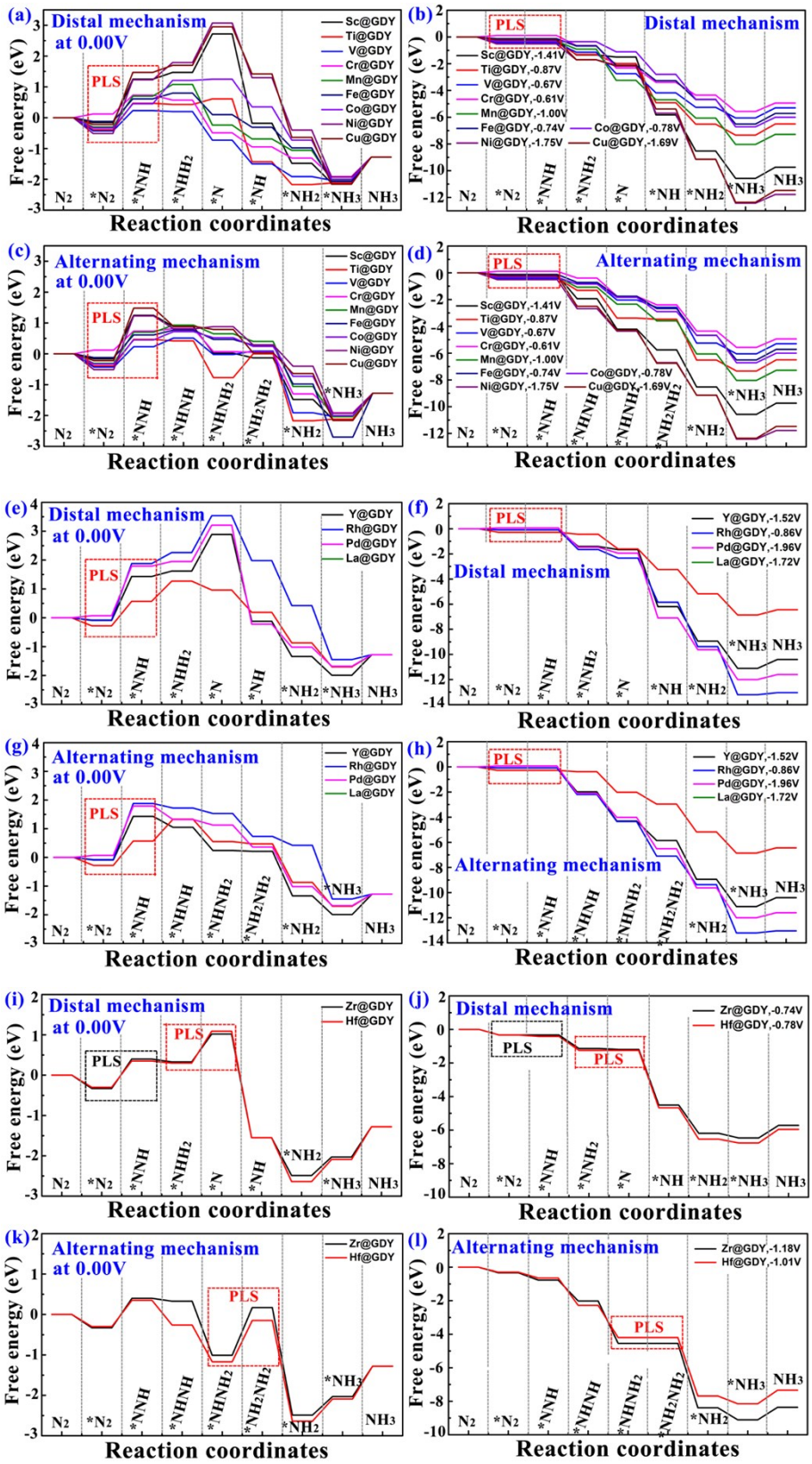

Fig. S6. Free-energy diagrams for N_2 reduction through distal (a) at 0.00 V and (b) at U_L, and alternating mechanisms (c) at 0.00 V and (d) at U_L on TM@GDY (TM=Sc,

Ti, V, Cr, Mn, Fe, Co, Ni, Cu) surfaces. Free-energy diagrams for N_2 reduction through distal (e) at 0.00 V and (f) at U_L, and alternating mechanisms (g) at 0.00 V and (h) at U_L on TM@GDY (TM=Y, Rh, Pd, La) surfaces. Free-energy diagrams for N_2 reduction through distal (i) at 0.00 V and (j) at U_L, and alternating mechanisms (k) at 0.00 V and (l) at U_L on TM@GDY (TM=Zr, Hf) surfaces.

Supplementary Tables

Table S1 Adsorption energies (E_{ads}, in eV) of N_2, NNH, and H_2O on the V@GDY 2×2 and 3×3 super cell.

Functional	Systems	E_{ads}, N_2 (end)	E_{ads}, NNH	E_{ads}, H_2O
PBE	V@GDY (2×2)	-0.88	-2.59	-0.80
PBE	V@GDY (3×3)	-0.90	-2.60	-0.81
PBE+U	V@GDY (2×2)	-0.85	-2.55	-0.72

In order to evaluate the effect of supercell, the adsorption energies of N_2, NNH, and H_2O on V@GDY in a 2×2 and 3×3 supercell were calculated and are shown in Table S3. The little difference of the computed adsorption energies suggest that the computed results are acceptable in this work.

In order to further evaluate the reliability of our results, PBE+U was conducted to re-examine the adsorption energies of N_2, NNH, and H_2O on V@GDY in a 2×2 supercell. The slight difference again shows that our results are acceptable in this work.

Table S2 Zero-point energy corrections (E_{ZPE}) and entropic contributions (at 298.15 K) to the free energies of the adsorbed species on TM@GDY estimated from the vibrational frequencies.

Species	ΔE_{ZPE}	$T\Delta S$
$*N_2$	0.1948	0.1340
*N-NH	0.4651	0.1433
$*N\text{-}NH_2$	0.8534	0.1273
*NH-NH	0.8108	0.1423
$*NH\text{-}NH_2$	1.1197	0.1742
$*NH_2\text{-}NH_2$	1.4782	0.2566
*N	0.0929	0.0498
*NH	0.3480	0.0909
$*NH_2$	0.6447	0.0144
$*NH_3$	1.0135	0.1413
N_2	0.15	0.58
H_2	0.27	0.41
NH_3	0.58	0.56

Table S3 Binding energy (E_b) of TM atom and GDY, cohesive energy of bulk metal (E_{coh}), energy difference (ΔE_b) between binding energy (E_b) and cohesive energy (E_{coh}), total magnetic moments (M_{tot}) and the amounts of charge (ΔQ) transmitted from the TM atoms to the GDY monolayers ('-' means losing electrons) of TM@ GDY structure.

Systems	Sc@GDY	Ti@GDY	V@GDY	Cr@GDY	Mn@GDY
E_b (eV)	6.49	6.39	5.33	3.92	4.11
E_{coh}(eV)	4.19	5.46	5.37	4.01	3.86
ΔE_b(eV)	2.30	0.93	-0.04	-0.08	0.25
ΔQ (e)	+1.43	+1.28	+1.04	+0.89	+0.83
$M_{tot}(\mu_B)$	0	1.15	2.55	3.64	3.54
Systems	Fe@GDY	Co@GDY	Ni@GDY	Cu@GDY	Zn@GDY
E_b (eV)	5.02	5.56	6.75	3.80	0.92
E_{coh}(eV)	4.78	5.36	4.90	3.51	1.12
ΔE_b(eV)	0.24	0.20	1.85	0.29	-0.20
ΔQ (e)	+0.50	+0.61	+0.49	+0.47	-
$M_{tot}(\mu_B)$	2.00	1.00	0	0	0
Systems	Y@GDY	Zr@GDY	Nb@GDY	Mo@GDY	Tc@GDY
E_b (eV)	6.85	7.39	6.34	4.78	5.58
E_{coh}(eV)	4.26	6.29	6.87	6.21	6.67
ΔE_b(eV)	2.59	1.09	-0.53	-1.43	-1.09
ΔQ (e)	-	-	-	-	-
$M_{tot}(\mu_B)$	0	1.07	2.51	2.44	3.08
Systems	Ru@GDY	Rh@GDY	Pd@GDY	Ag@GDY	Cd@GDY
E_b (eV)	5.98	5.82	4.42	2.55	1.95
E_{coh}(eV)	6.15	5.89	3.74	2.35	5.19
ΔE_b(eV)	-0.17	-0.07	0.68	0.20	-3.24
ΔQ (e)	-	-	+0.71	-	-
$M_{tot}(\mu_B)$	0	1.00	0	0	0
Systems	La@GDY	Hf@GDY	Ta@GDY	W@GDY	Re@GDY
E_b (eV)	7.57	7.14	6.92	6.31	5.95
E_{coh}(eV)	4.32	6.44	8.28	8.42	7.58
ΔE_b(eV)	3.25	0.70	-1.36	-2.11	-1.63
ΔQ (e)	-	-	-	-	-
$M_{tot}(\mu_B)$	0	1.07	2.08	1.79	1.00
Systems	Os@GDY	Ir@GDY	Pt@GDY	Au@GDY	Hg@GDY
E_b (eV)	6.63	6.31	5.82	2.46	1.29

E_{coh}(eV)	7.74	7.21	5.71	2.86	1.67
ΔE_b(eV)	-1.11	-0.90	0.12	-0.40	-0.38
ΔQ (e)	-	-	+0.11	-	-
$M_{tot}(\mu_B)$	0	1.00	0	0	0

Table S4 The calculated limiting potentials (U_L in V) and PLS for the different catalysts that have been synthesized very recently.

Systems	Pathway	PLS	U_L (V)	References
V@GDY	**Distal/ Alternating**	**$*N_2+H^++e^-\rightarrow *NNH$**	**-0.67**	**Present work**
Ti@GDY	Distal/ Alternating	$*N_2+H^++e^-\rightarrow *NNH$	-0.87	Present work
Fe@GDY	Distal/ Alternating	$*N_2+H^++e^-\rightarrow *NNH$	-0.74	Present work
Co@GDY	Distal/ Alternating	$*N_2+H^++e^-\rightarrow *NNH$	-0.78	Present work
Zr@GDY	Distal	$*N_2+H^++e^-\rightarrow *NNH$	-0.74	Present work
Rh@GDY	Distal/ Alternating	$*N_2+H^++e^-\rightarrow *NNH$	-0.86	Present work
Hf@GDY	Distal	$*NNH_2+H^++e^-\rightarrow *N+NH_3$	-0.78	Present work
Co_2@GDY	Distal	$*NH_2+H^++e^-\rightarrow *NH_3$	-0.43	Ma et al. 2019[3]
Nb_2O_5 (181)	Distal	$*NNH_2+H^++e^-\rightarrow *N+NH_3$	-0.56	Han et al. 2018[4]
Defect-rich MoS_2	Distal	$*NH_2+H^++e^-\rightarrow *NH_3$	-0.60	Li et al. 2018[5]
Ru_1-N_3	Distal	$*N_2+H^++e^-\rightarrow *NNH$	-0.73	Li et al. 2018[6]
Ru_1-N_4	Distal	$*N_2+H^++e^-\rightarrow *NNH$	-0.77	Li et al. 2018[6]
MoS_2 with Mo edge	Distal	$*N_2+H^++e^-\rightarrow *NNH$	-0.68	Zhang et al. 2018[7]
Mo_2C (111)	Distal	$*N_2+H^++e^-\rightarrow *NNH$	-0.74	Ren et al. 2019[8]
Mo_2C (002)	Distal	$*NH_2+H^++e^-\rightarrow *NH_3$	-0.92	Chen et al. 2018[9]
Ru(0001)	Distal	$*N_2+H^++e^-\rightarrow *NNH$	-0.94	Skulason et al. 2012[10]
Ru_1@C_2N	Distal/ Alternating	$*N_2+H^++e^-\rightarrow *NNH$	-0.96	Cao et al. 2018 [11]
W@N-doped graphyne	Distal	$*N_2+H^++e^-\rightarrow *NNH$	-0.29	He et al. 2019[12]
V/ β_{12} boron monolayer	-	$*N_2+H^++e^-\rightarrow *NNH$	-0.28	Zhu et al. 2019[13]
Mo_1-N_1C_2	Enzymatic	$*N_2+H^++e^-\rightarrow *NNH$	-0.40	Lin et al. 2018[14]
Mo-embedded BN monolayer	Enzymatic	$*NH_2+H^++e^-\rightarrow *NH_3$	-0.35	Zhao et al. 2017[15]
Mo^0/GDY	Alternating	$*NHNH+H^++e^-\rightarrow *NHNH_2$	-0.71	Hui et al. 2019[16]

References

1 Zhen Feng, Renyi Li, Yaqiang Ma, Yi Li, Dong Wei, Yanan Tang, Xianqi Dai. Molecule-level graphdiyne coordinated transition metals as a new class of bifunctional electrocatalysts for oxygen reduction and oxygen evolution reactions. Physical Chemistry Chemical Physics, 2019, 21, 19651-19659.

2 Zhen Feng, Yanan Tang, Weiguang Chen, Dong Wei, Yaqiang Ma, Xianqi Dai. O-doped graphdiyne as metal-free catalysts for nitrogen reduction reaction. Molecular Catalysis 2020, 483,110705.

3 Dongwei Ma, Zeng Zaiping, Liu Liangliang, et al. Computational evaluation of electrocatalytic nitrogen reduction on TM single-, double-, and triple-atom catalysts (TM = Mn, Fe, Co, Ni) based on graphdiyne monolayers. The Journal of Physical Chemistry C, 2019, 123(31), 19066-19076.

4 Jingrui Han, Liu Zaichun, Ma Yongjun, et al. Ambient N_2 fixation to NH_3 at ambient conditions: Using Nb_2O_5 nanofiber as a high-performance electrocatalyst. Nano Energy, 2018, 52, 52264-270.

5 Xianghong Li, Li Tingshuai, Ma Yongjun, et al. Boosted electrocatalytic N_2 reduction to NH_3 by defect-rich MoS_2 nanoflower. Advanced Energy Materials, 2018, 8(30), 1801357.

6 Zhigang Geng, Liu Yan, Kong Xiangdong, et al. Achieving a record-high yield rate of 120.9 μg NH_3 mg cat.$^{-1}$ h^{-1} for N_2 electrochemical reduction over Ru single-atom catalysts. Advanced Materials, 2018, 30(40), 1803498.

7 Ling Zhang, Ji Xuqiang, Ren Xiang, et al. Electrochemical ammonia synthesis via nitrogen reduction reaction on a MoS_2 catalyst: Theoretical and experimental studies. Advanced Materials, 2018, 30(28), 1800191.

8 Xiang Ren, Zhao Jinxiu, Wei Qin, et al. High-performance N_2-to-NH_3 conversion electrocatalyzed by Mo_2C nanorod. ACS Central Science, 2019, 5(1), 116-121.

9 Hui Cheng, Ding Liang-Xin, Chen Gao-Feng, et al. Molybdenum carbide nanodots enable efficient electrocatalytic nitrogen fixation under ambient conditions. Advanced Materials, 2018, 30(46), 1803694.

10 Egill Skúlason, Bligaard Thomas, Gudmundsdóttir Sigrídur, et al. A theoretical evaluation of possible transition metal electro-catalysts for N_2 reduction. Physical Chemistry Chemical Physics, 2012, 14(3), 1235-1245.

11 Yongyong Cao, Gao Yijing, Zhou Hu, et al. Highly efficient ammonia synthesis electrocatalyst: Single Ru atom on naturally nanoporous carbon materials. Advanced Theory and Simulations, 2018, 18000181-10.

12 Tianwei He, Sri Kasi-M, Du Aijun. Single tungsten atom supported on N-doped graphyne as a high-performance electrocatalyst for nitrogen fixation under ambient conditions. Physical Chemistry Chemical Physics, 2019, 21, 1546-15551.

13 Hao-Ran Zhu, Hu Yan-Ling, Wei Shi-Hao, et al. Single-metal atom anchored on boron monolayer (β_{12}) as an electrocatalyst for nitrogen reduction into ammonia at ambient conditions: A first-principles study. The Journal of Physical Chemistry C, 2019, 123(7), 4274-4281.

14 Chongyi Ling, Bai Xiaowan, Ouyang Yixin, et al. Single molybdenum atom anchored on N-doped carbon as a promising electrocatalyst for nitrogen reduction into ammonia at ambient conditions. The Journal of Physical Chemistry C, 2018, 122(29), 16842-16847.
15 Jingxiang Zhao, Chen Zhongfang. Single Mo atom supported on defective boron nitride monolayer as an efficient electrocatalyst for nitrogen fixation: A computational study. Journal of the American Chemical Society, 2017, 139(36), 12480-12487.
16 Lan Hui, Xue Yurui, Yu Huidi, et al. Highly efficient and selective generation of ammonia and hydrogen on a graphdiyne-based catalyst. Journal of the American Chemical Society, 2019, 141(27), 10677-10683.